Journal of Applied Geophysics 72 (2010) 57–69

Contents lists available at ScienceDirect

Journal of Applied Geophysics

journal homepage: www.elsevier.com/locate/jappgeo

P and PS data to reduce the uncertainty in the reconstruction of near-surface alluvial deposits (Case study—Central Italy)

Luciana Orlando *, Giovanni Pelliccioni

Dept. Idraulica, Trasporti e Strade- Sapienza University of Rome, Italy

ARTICLE INFO

Article history:
Received 6 November 2008
Accepted 1 July 2010

Keywords:
Seismic reflection
P and PS waves
Seismic refraction
Electrical resistivity data
Multi-array surficial waves
Joint data interpretation

ABSTRACT

Seismic refraction, surface wave surveys and P and PS seismic reflection data were acquired and processed to derive the geological setting as well as P and S velocity profiles of the Plio–Pleistocene sediments that are filling a tectonic valley in central Italy. The results were constrained by boreholes, vertical electrical sounding and electrical resistivity tomography. The P-wave data, processed with standard processing, was allowed to detect the top of limestone 50 m depth. The converted PS-wave data were processed with Asymptotic Common Conversion Point (ACCP) sort and non-hyperbolic normal move out correction. The study shows that special care must be devoted to data muting because of the low signal-to-noise ratio, which is mainly due to the high energy of the ground roll and the air wave. The stack section was the result of an iterative process. From theoretical analysis, we determined that the use of ACCP binning does not allow the reflection to be focused for all of the time windows because the ACCP approximation is correct only for depths greater than the shot-receiver offset.

The joint interpretation of the direct and indirect data proved the capability of P and PS seismic reflection data of constraining the interpretation and removing the ambiguity in the reconstruction of the geological setting and the P and S profiles of the formation of an alluvial valley located in a seismic area.

Contents

1. Introduction

In the evaluation of the seismic and hydro-geologic risk, the knowledge of lithologies, thicknesses and elastic low-strain properties of the near-surface formations is becoming increasingly important. In the last few years, the use of geophysical methods to obtain this kind of information has become more common (Cardarelli et al., 2007). To reduce the intrinsic uncertainty of each single technique, several geophysical methods are applied, and the data are jointly inverted and with *a priori* constraints obtained from borehole data. Vertical electrical soundings (VES), electrical resistivity tomography (ERT), seismic refraction, Multichannel Analysis of Surface Waves (MASW)

* Corresponding author. Tel.: +0039 06 44585078; fax: +0030 06 44585080.
E-mail address: luciana.orlando@uniroma1.it (L. Orlando).

0926-9851/$ – see front matter © 2010 Elsevier B.V. All rights reserved.
doi:10.1016/j.jappgeo.2010.07.002

(Xia et al., 1999; Socco and Strobbia, 2004) and down and cross-hole seismic methods (Bernabini and Cardarelli, 1997; Hunter et al., 2002) are usually used to determine P and S velocity profiles and to reconstruct the near-surface features. The P-wave velocity is determined from seismic refraction and down and cross-hole seismic measurements, and S-wave velocity is determined from MASW, down and cross-hole seismic measurements.

In hydrocarbon exploration, P- and S-wave profiles (Hilterman, 2001; Yilmaz, 2001; Domenico, 1974) are used to determine physical properties of rocks such as lithology, porosity, pore fill, anisotropy, etc.

More recently, S-wave profiles for near-surface studies have been examined through pure shear (SH) seismic survey (Deidda and Balia, 2001, Young and Hoyos, 2001) and converted waves (PS) (Carr and Hajnal, 1999; Carr et al., 1998; Schafer, 1993; Yang, 2003; Harris et al., 2000).

In this paper, we analyse the capability of seismic data, i.e., seismic refraction, MASW, P and PS seismic data, to reconstruct the near-surface formations and to determine P and S velocity profiles for microzonation studies. The study area is located in central Italy very near to the epicentre of the 6.3 magnitude earthquake that occurred April 6, 2009 in L'Aquila town. Seismic data are jointly interpreted with VES, electrical resistivity tomography and boreholes.

2. Theoretical framework

Among the various seismic methods, the PS converted wave processing is a very challenging task, requiring several modifications with respect to the P-wave processing due to the asymmetry of the source-to-receiver ray. It is well known that PS converted waves are generated at the boundary layer by a compressional (P) wave for non-normal incidence (Yilmaz, 2001). In the absence of out-of-plane scattering and velocity anisotropy, the PS-wave raypath is asymmetric due to the slower velocity of S than P-waves (Fig. 1).

The use of converted waves in exploration geophysics gained popularity only in the 1980s, even though shear-wave recording can be traced back to earthquake studies in the 1800s. The first use of converted waves (PS) for exploration purposes was by Garotta and Granger (1988). Iverson et al. (1989), derived the Vp/Vs ratio from the stacking velocities of the P and PS data, and Nazar (1991) demonstrated the possibility of using PS data for lithology identification through amplitude-versus-offset (AVO) analysis.

PS waves have several potential advantages over SH waves, including:

- The significantly reduced acquisition cost because they do not require a special source;
- Attenuation of the shear waves in the near-surface is only present for the up-going ray path, rather than both down-going and up-going paths;

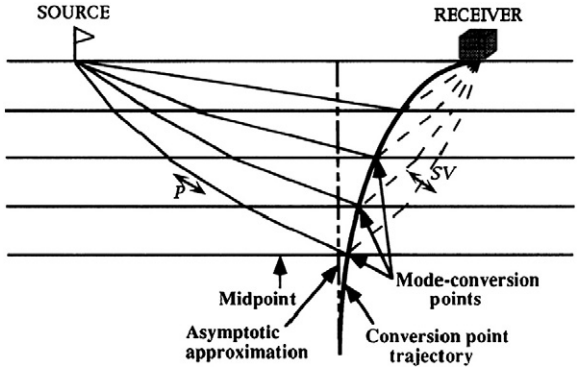

Fig. 1. PS-wave raypath asymmetry: CCP point changes with the depth (Yilmaz, 2001).

- The reduced near-surface static delay, which only needs to estimate the residual receiver static.

The major disadvantages of PS data are:

- Complicated processing required due to the asymmetry of the source-to-receiver ray path;
- The difficulty of S-wave velocity estimation.

Beyond conventional processing, the most difficult issues of PS data are:

1. The receiver static correction;
2. The velocity profile evaluation;
3. CCP binning.

The source-to-receiver raypath makes CCP sorting quite difficult because the common reflection point (*XP*) is laterally shifted towards the receiver, depending on the depth and velocity ratio $\gamma = Vp/Vs$.

Since γ is generally unknown, an asymptotic common conversion point (ACCP) binning approximation is often used (Li and Lu, 1999) instead of CCP binning (Zhang and Robinson, 1992; Zhang, 1996; Yuan and Li, 1997; Tessmer and Behle, 1988). This approximation is correct only for a source-receiver offset that is shorter than the reflector depth as shown below.

For a homogeneous flat layer with a width of H and with Vp and Vs velocities, the CCP location can be determined by taking into account a reflected raypath with a ϑp incident angle and a ϑs reflected angle and indicating with *Xp*, D and H the horizontal distance between the source location and the conversion point, the source-receiver offset and the depth of layer, respectively (Thomsen, 1999):

$$Xp = \frac{D\cos(\vartheta s)}{\gamma\cos(\vartheta p) + \cos(\vartheta s)} \tag{1}$$

where $\gamma = \frac{Vs}{Vp}$.

For $H \to \infty$, both ϑp and $\vartheta s \to 0$, and the relation (1) becomes:

$$\frac{Xp}{D-Xp} = \frac{\tan(\vartheta p)}{\tan(\vartheta s)} = \frac{Vp\cos(\vartheta s)}{Vs\cos(\vartheta p)} = \gamma\frac{\cos(\vartheta s)}{\cos(\vartheta p)} \to \frac{Vp}{Vs} = \gamma \tag{2}$$

The ACCP is given by:

$$Xp = \frac{D_\gamma}{1+\gamma} = \frac{D}{1+\gamma'} \tag{3}$$

Expression (3) indicates the asymptotic location of the conversion point (ACCP) under the condition of ϑp, $\vartheta s \to 0$ for $H \to \infty$. Note that the ACCP offset (3) between two consecutive receivers is the same for each depth and γ, while the CCP offset (1) under the same condition depends on the source-receiver offset. Therefore, the use of ACCP is correct only for $D/H \to 0$, i.e., for deep layers and not for those near the surface.

To evaluate the errors induced by the ACCP approximation for near-surface layers, we compare *Xp* values calculated with relation (1) and (3) for $\gamma = Vp/Vs = 1.5, 2, 2.5$ and depth layers of 20, 40, 60, 80 and 100 m. The receiver offset was 1 m, the shot-receiver offset was 11 m and the receiver number was 48. In Fig. 2, the differences between CCP and ACCP offsets versus ACCP offset are mapped. The graphs show that the difference is inversely proportional to γ and increases nonlinearly as the shot-receiver offset increases; for a 20 m-deep layer, the maximum difference between CCP and ACCP offsets is more than three times the receiver offset.

The above consideration shows that the use of the ACCP approximation is not appropriate for reflectors shallower than shot-receiver offsets. In this case, it needs an appropriate code that allows the traces to be binned in the correct manner for each depth; otherwise, only the reflection responding to the actual γ is focused.

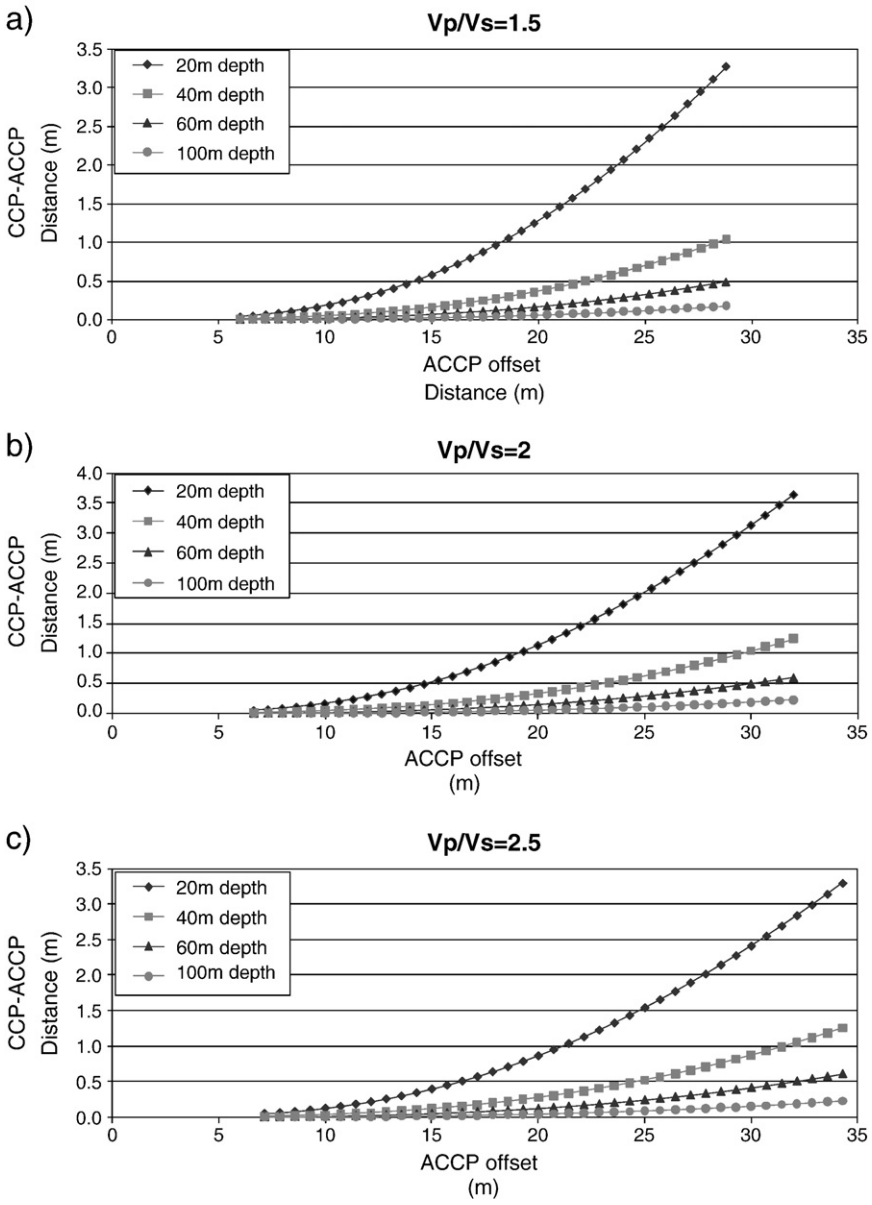

Fig. 2. Map of difference between CCP and ACCP versus ACCP offsets for $\gamma = 1.5$, 2, 2.5 and depth layers of 20, 40, 60, 80 and 100 m.

3. Geology and background of geophysical data

The study area is located in central Italy (Fig. 3) about 6 km northwest of L'Aquila. The area consists of a complex tectonic valley filled by Plio–Pleistocene sediments lying on limestone bedrock outcropping in the mountains (Fig. 3). The geological profile transversing the valley axis (Fig. 4) shows a bedrock tectonically detached with the main fault straight on the valley axis. The bedrock formed by limestone was drilled by boreholes (Fig. 5) only at the edge of the valley.

The boreholes (25–52 m in depth) show that the near-surface sediments consist mainly of alluvial deposits formed by sand, gravel, silt and clay. The boreholes BH1, BH2, BH3, BH4 and BH7 (Fig. 5) located near the edge of the valley have reached the bedrock formed by limestone at a depth of 25–51 m, while the depth of bedrock is unknown at the centre of the valley as it was never investigated with boreholes.

A stratigraphy (Fig. 6a) along the two-dimensional profile located normally to the valley axis (Fig. 4) was carried out from 20 vertical electrical soundings (VES) whose inversions were constrained up to 50 m with stratigraphy of 7 boreholes.

In Fig. 6b, a two-dimensional electrical resistivity tomography (ET3 in Fig. 5) profile, located (Fig. 4) more or less in the same position of the VES profile, is shown.

Comparison of the VES and ERT profiles in Fig. 6a and b shows a very similar setting of the near-surface electrical stratigraphy. The VES profile clearly shows the lateral discontinuity of resistive strata (layers 1 and 2 in Fig. 6a) located between VES16 and 15 and the overlapping of a resistive layer 2 to a conductive layer 3. This was not so clearly highlighted with ERT, probably due to the low resolution and interpolation of the data.

The joint interpretation of VES, ERT and borehole data allowed the low resistivity near-surface formation (20 to 200 Ω·m) to be interpreted as alluvial deposits formed by clay-silt, sand and gravel, and layer 1 as limestone. Because layers 2 and 3 were not investigated with boreholes, they were interpreted only on the basis of the electrical survey. For layer 2, with a resistivity of 600 Ω·m, we advanced the hypothesis that it could be associated with compacted

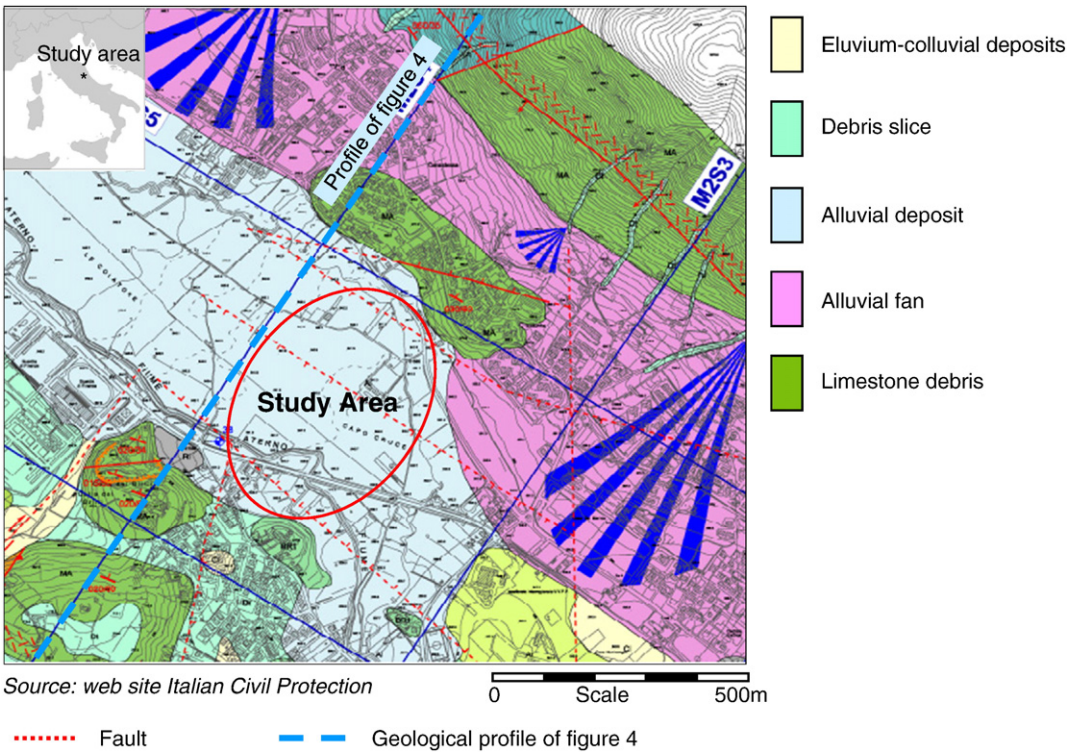

Fig. 3. a) Study area location. b) Geological map and study area.

gravel formation or a detached limestone slab, and layer 3 could be a clay formation.

4. Seismic data

4.1. Seismic data acquisition

The area was surveyed with two MASW profiles, three seismic refraction profiles, two P-wave seismic reflection profiles and one PS converted wave seismic reflection profile (Fig. 5).

Generally, the near-surface seismic reflection data are characterised by a low signal-to-noise ratio due to the overlap of ground roll, head and air waves compared to the reflected waves (Feroci et al., 2000). Therefore, to increase the signal-to-noise ratio, it is of utmost importance to take much care the receiver and source setting of the data acquisition so to acquire the reflection data inside the optimum windows (Hunter et al., 1982).

In the case study, to define the optimum window for shallow reflection survey, a P-wave synthetic arrival times was generated (Fig. 7). The theoretical shot gather, which included P reflections as well as refracted and direct ground and air waves, is calculated for offsets from 0 to 100 m. The shot was simulated for horizontal layers with root mean square velocities of 400, 750, 820 and 1600 m/s and depths of 4, 20, 50 and 80 m, respectively; such parameters were designed as a good approximation of the actual setting of the study area. In the simulation, the direct air and ground waves (Fig. 7) are the upper limit of the ground roll of a single frequency with a linear ray path and velocity of 300 m/s. Fig. 7 shows that in the near-surface zone, the optimum window area is very small, and the reflection from the first layer is entirely outside of the optimum window while the reflections from the others lie within the optimum windows only for

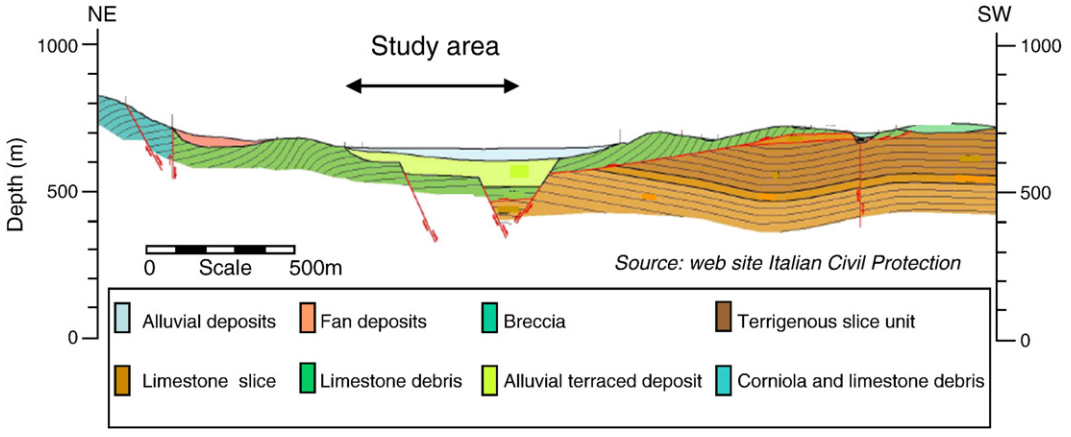

Fig. 4. Geological profile transversing the valley axis. Location in Fig. 3b.

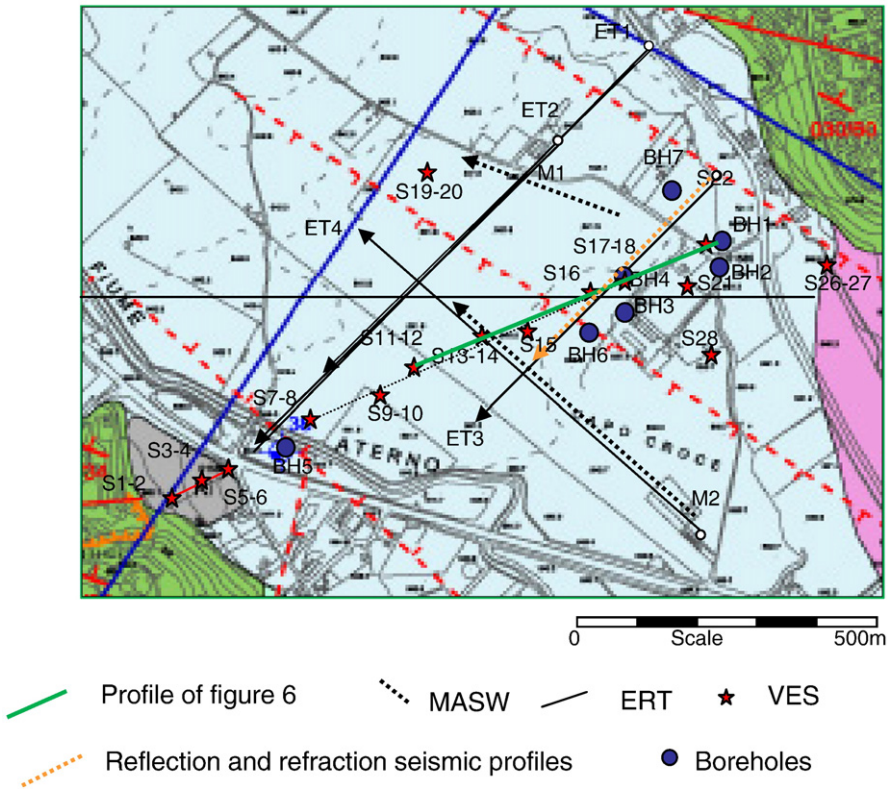

Fig. 5. Location of direct and indirect surveys.

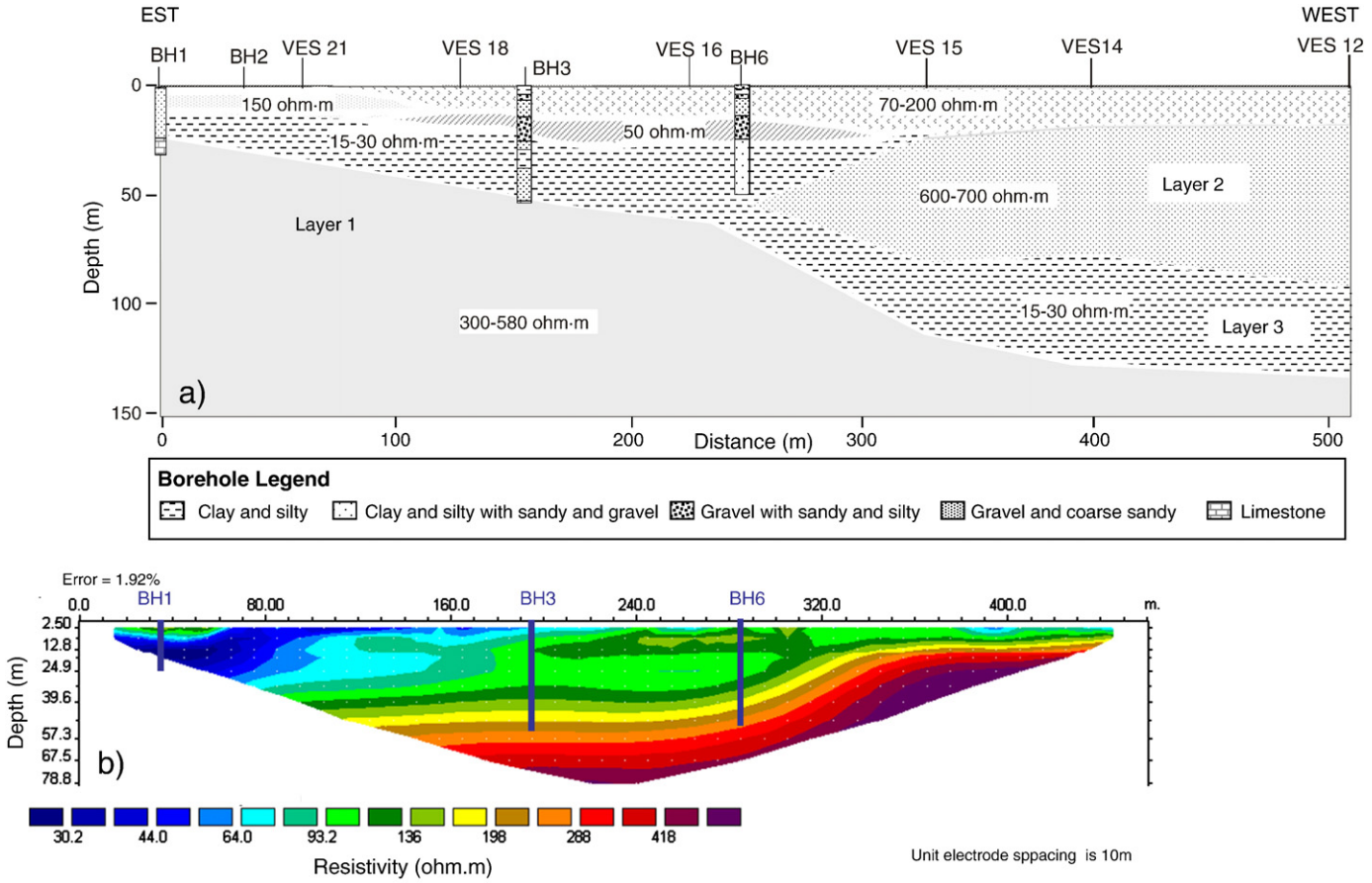

Fig. 6. Two-dimensional section located transversing the valley axis (for location see geological map in Fig. 4) obtained with the joint interpretation of VES and boreholes data (a). Electrical resistivity tomography (b) (ET3 in Fig. 5).

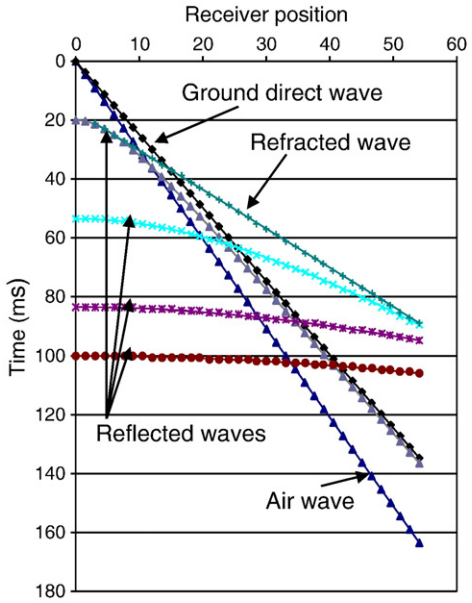

Fig. 7. Synthetic P-waves shot generated for a 4 horizontal layer model with root mean square velocities of 400, 750, 820 and 1600 m/s, and interfaces depth of 4, 20, 50 and 80 m.

wide-angle reflections. Moreover, the refracted wave overlaps the near-surface reflections, and the overlap increases for wide-angle reflections. Therefore, in this study, the shot and geophone offset was chosen carefully because only a limited number of channel recording instruments were available.

Based on previous theoretical results and on experiments (Feroci et al., 2000), where data with different offsets were acquired and analysed to prove that the traces with short shot geophone offsets are characterised by very low signal-to-noise ratios, geophone and shot offsets were chosen such that they remained at a maximum inside the optimum windows.

The seismic reflection and refraction profiles were collected approximately parallel to the ET3 section shown in Fig. 6 (for location see Fig. 5). In detail, two P and one PS seismic reflection as well as three seismic refraction lines were gathered (Fig. 5).

The two P-wave lines and the PS-wave line were 186 m, 306 m and 71 m long, respectively.

The shots of seismic profiles were off-end, and P1 and P2 lines were acquired with different shots and geophone offsets to relate the investigation depth and quality of data with the geometry of the seismic lines. Details of the acquisition parameters are shown in Table 1. The geometries of P1 and P2 lines were chosen for the purpose of assisting the near-surface and deep reflections, respectively. The P vertical component and the in-line radial component (PS) of the ground motion were not simultaneously recorded.

On the P2 line, three seismic refraction profiles were collected with the aim of detailing the P-wave velocity and setting of the near-surface layers, as well as carrying out the delay time for the seismic static correction.

The seismic refraction profiles were acquired with 48 receivers with an offset of 1.5 m. On each profile, seven shots at −30, 0, 17.625, 35.25, 52.875, 70.5 and 100.5 m were fired.

The two MASW (M1 and M3 in Fig. 5) arrays were collected parallel to the valley axes. The M1 and M2 arrays are 220 and 440 m long with receiver offsets of 10 m. The former array is located about 200 m north-east of the M2 array.

A 48-channel seismograph "Geode" (EG&G Geometrics) with a 24-bit A/D conversion capability was used for the seismic data acquisition. The source of seismic refraction and reflection surveys was a Minibang shotgun (eight-gauge) fired downhole at a depth of about 0.20 m. The receivers were Mark Products with a proper frequency of 40 Hz for the P-seismic reflection and refraction profiles and of 4.5 Hz for the PS seismic reflection profile.

The MASW arrays were acquired with 24 channels and with 2048 samplings per scan. Each receiver point was equipped with vertical and horizontal sensors with central frequencies of 4.5 Hz. The source was a weight drop of about 700 kg, which had fallen from 1.5 m above the topographic level by the crane of a truck.

4.2. Data processing and analysis

4.2.1. Seismic refraction

The refraction data were processed to compute static correction and to reconstruct the near-surface seismic stratigraphy. The first break was manually picked and used in the evaluation of velocities and layer numbers. The inversion for seismic stratigraphy reconstruction was obtained with Cat3D code commercialized by OGS (Italy) based on the SIRT (Simultaneous Iterative Reconstruction Technique) algorithm.

The refraction profile (Fig. 8) revealed three layers with meanly velocities of 500, 900 and 2200 m/s:

1. The first near-surface layer has a velocity of about 500 m/s and a thickness ranging from 2 to 4.5 m;
2. The second layer has a velocity around 900 m/s and a thickness ranging from 3 to 6–7 m;
3. The third layer has a velocity of 1900–2500 m/s.

By comparing the results of the seismic refraction data with boreholes BH7, BH3, BH4 and BH6, the near-surface seismic layer of 2–5 m in thickness and velocity of 500 m/s was associated with the colluvial deposits and/or sandy-clay debris; the second layer, with a wave velocity around 900 m/s and thickness around 4–6 m, was associated to slimy-clay with pebbles and slimy-gravel with sand; and the third layer, with a mean velocity of 2200 m/s, was associated with compacted gravel and sand.

Analysis of the first breaks of MASW data shows a refractor with a depth of 45–50 m and a velocity of around 3000–3100 km/s, which fit well with the top of limestone (Orlando et al., 2003). This refractor was not detected by previous refraction surveys because of the small length of the refraction profile and short shot-receiver offest.

4.2.2. MASW

The MASW data processing was performed using the inversion code developed by Rix et al. (2000). The code assumes elasticity of media and independence of the solution of the inverse problem from the damping ratio of the surface wave. The data inversion was constrained with the borehole data.

The MASW seismic velocity profile of the M1 array is shown in Fig. 9. The velocity range is from 230 to 1340 m/s with velocity inversion occurring at a depth of 24 m. By comparing the velocity profile with the data borehole BH7, we associated the near-surface layer with a velocity of 230 m/s to the formation formed by colluvial deposits, slimy-clay, slimy-gravel and sand; the second layer, with a velocity of 960 m/s and thickness of 6.3 m, was associated with

Table 1
Geometries of P and PS waves data acquisition.

	P-wave line 1	P-wave line 2	PS-wave line 3
Channel	36	36	24
Geophone offset	1 m	1.5 m	1.5 m
Shot interval	1 m	1.5 m	1.5 m
Shot offset	10 m	19.5 m	19.5 m
Record length	0.5 s	0.5 s	0.5 s
Sample interval	0.5 ms	0.25 ms	0.25 ms
Fold	1800%	1800%	1200%

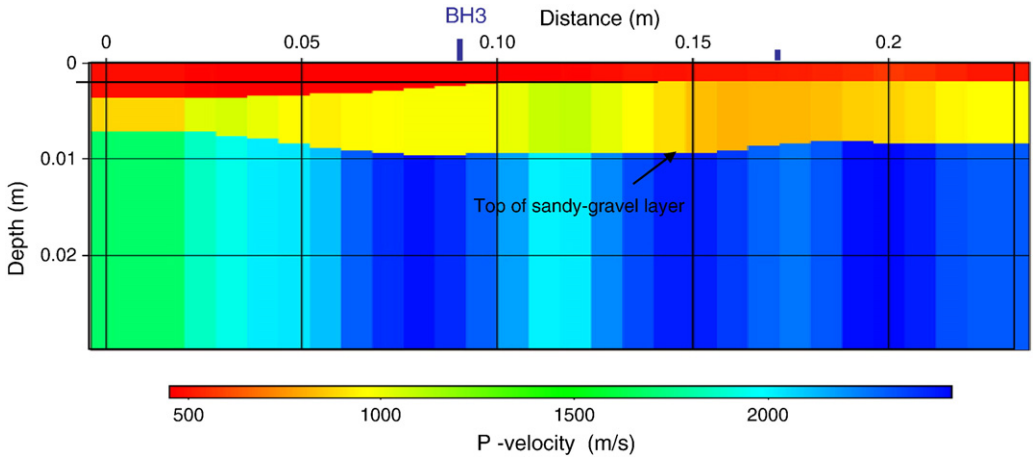

Fig. 8. Seismic refraction profile acquired on P-seismic reflection data.

compacted gravel and sand; the third layer with a velocity of 400 m/s and thickness of 12.7 m was associated with sandy-clay and the forth layer with a velocity of 1340 m/s was associated with limestone. The velocity inversion occurs at the interface between the bottom of a compacted gravel and sand layer and the top of a clay-sand layer.

P and S velocities determined from seismic refraction and MASW data combined with BH3 borehole stratigraphy were used to provide two-way travel times of the P, S and PS velocity profiles in correspondence with the seismic reflection profiles (Fig. 10) These profiles were used for initiating the inversion and interpretation of P and PS stack sections.

4.2.3. P-wave seismic reflection

The P and PS seismic reflection data were processed with the SPW—Seismic Processing Workshop of the Parallel Geosciences Corporation.

The processing of the P-wave data consisted of shot editing, noise suppression and polarity change of inverse polarity traces, static corrections, coherent-noise muting, filtering, CMP sorting, residual static correction, normal move out (NMO) corrections and stacking.

The processing parameters were chosen on the basis of the data and spectral analysis, which are summarised below.

The P-wave shot (Fig. 11) looks quite similar to the theoretical shot (Fig. 7), confirming that the signal-to-noise ratio is high only

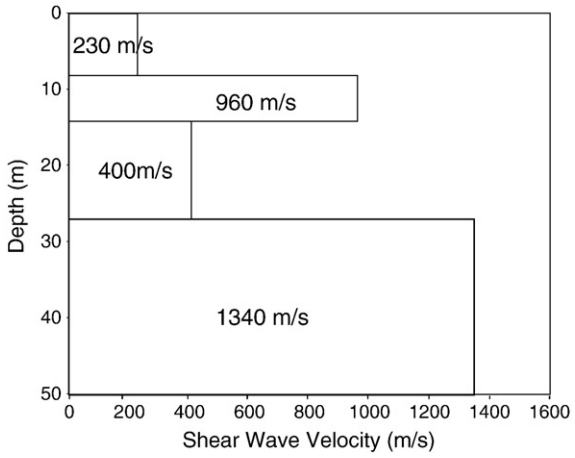

Fig. 9. MASW data with inversion constrained with borehole stratigraphy.

out of the ground roll cone in both P1 and P2 lines. Spectral analysis of the shots shows amplitudes $> -17 \div 20$ dB between 40 and 95 Hz for the P1 line (Fig. 12a) and between 40 and 120 Hz for the P2 line (Fig. 12b). The P2 line has 2 peak frequencies at 55 and 110 MHz. For both lines, the peak noise frequencies are between 35–50 Hz with amplitudes $> -14 \div 16$ dB from 20 to 60 Hz (Fig. 12b). The P1 and P2 line signals have frequencies up to 140 and 180 Hz, respectively, with amplitudes > -14 dB (Fig. 12c). The P2 line, acquired with a receiver offset of 1.5, shows a wider band frequency and a greater signal-to-noise ratio than the P1 line. For a frequency of 180 Hz and a P-wave velocity of 2000 m/s, a theoretical resolution of 2.8 m (Rayleigh criterion of $\lambda/4$) is estimated.

To increase the signal-to-noise ratio, we applied to the data a severe muting of the ground roll and the refracted wave and a bandpass time filter (10–50 Hz to 250–400 Hz). The velocity profile for the normal move out correction was attained by fitting hyperbolae to reflections of CMP gather**.** To improve the quality of the stacked section, residual static corrections were estimated and applied before to the stack itself. The static corrections were calculated in two different ways: the first one from the seismic refraction, using the delays under each geophone and shot with the intercept method (Gardner, 1939; Bernabini, 1965) and the second one by automatic picking of first arrivals of the seismic refraction events along with subsequent manual revision. We obtained sections that were quite similar.

The P1 and P2 stack sections are shown in Fig. 13. Depending on the receiver offset, which was 1 m for the first line and 1.5 m for the second line, P1 and P2 profiles were found to be 100 and 200 ms, respectively. The sections show that shot offset influences the ability of seismic reflection to investigate the near-surface zone; in fact, the P1 profile acquired with a shot offset of 10 m has reflections above 15 ms, and the P2 profile with a 19.5 m shot offset has reflections above 30 ms. The sections show many more or less discontinuous reflections, and the most important are marked with dotted lines. The P two-way travel time of Fig. 10b, drawn in Fig. 13 near the borehole BH3, indicates that reflection 1, at 27 ms, is related to the top of the compacted sandy-gravel formation. This reflector was better detected by line P1, depending on the shot-receiver offset. Reflection 2, detected by both lines, is related to the top of limestone. The former reflection, at a depth varying from 40 to 60 ms, appears discontinuous mainly at CMP 120 of the P1 line (60 m from the start line) and at CMP 220 of the P2 line. Starting from CMP240 of P2, the reflection appears with higher continuity and reflectivity. Referring to the geologic map and section of Figs. 3 and 4, we correlated the lateral discontinuity of reflector 2 to the fault system reported by Tallini and Magaldi (2002). The seismic section indicates that

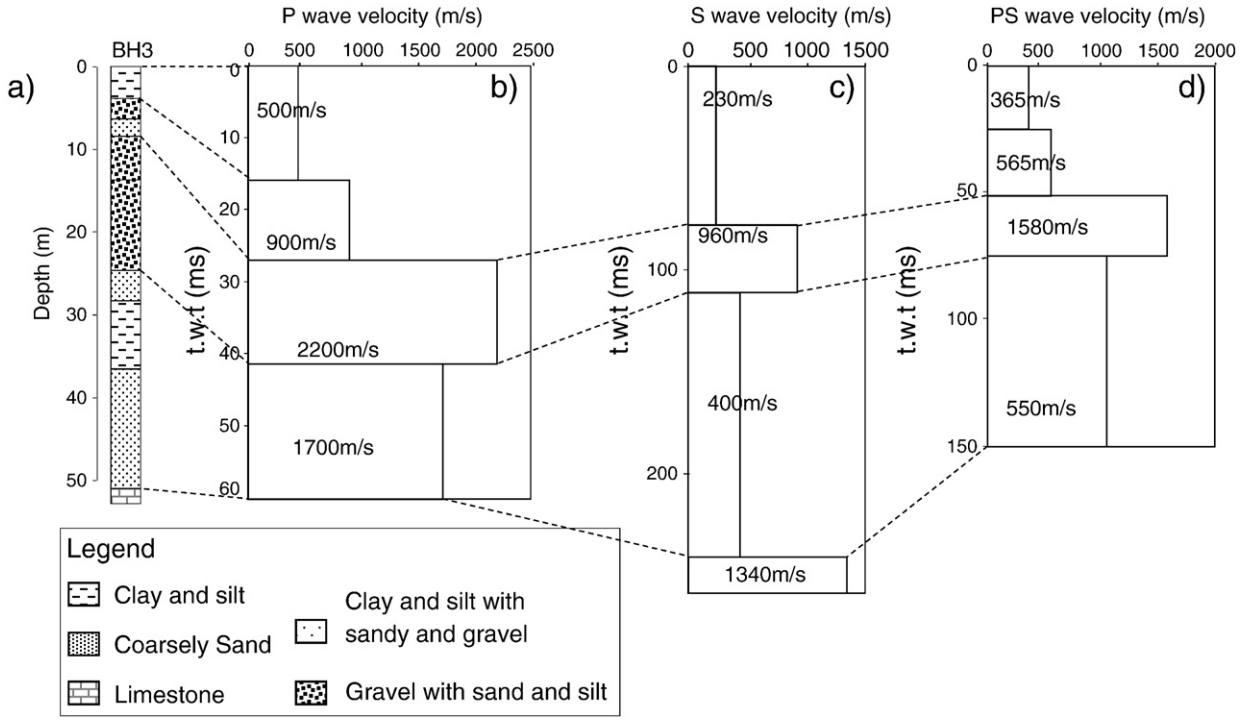

Fig. 10. a) Borehole BH3 stratigraphy. b) P velocity two-way travel time profile. c) S velocity two-way travel time profile. d) PS velocity two-way travel time profile obtained combining P and S velocity profiles.

between CMP20 and 200 there is a system normal fault, which gradually pushes the limestone toward the centre of the valley. The raising of the limestone from CMP220 can be interpreted as a reverse fault and/or thrust rather than a direct fault as indicated in the geological section of Fig. 4. Reflections into the limestone indicate that it consists of a stratified formation.

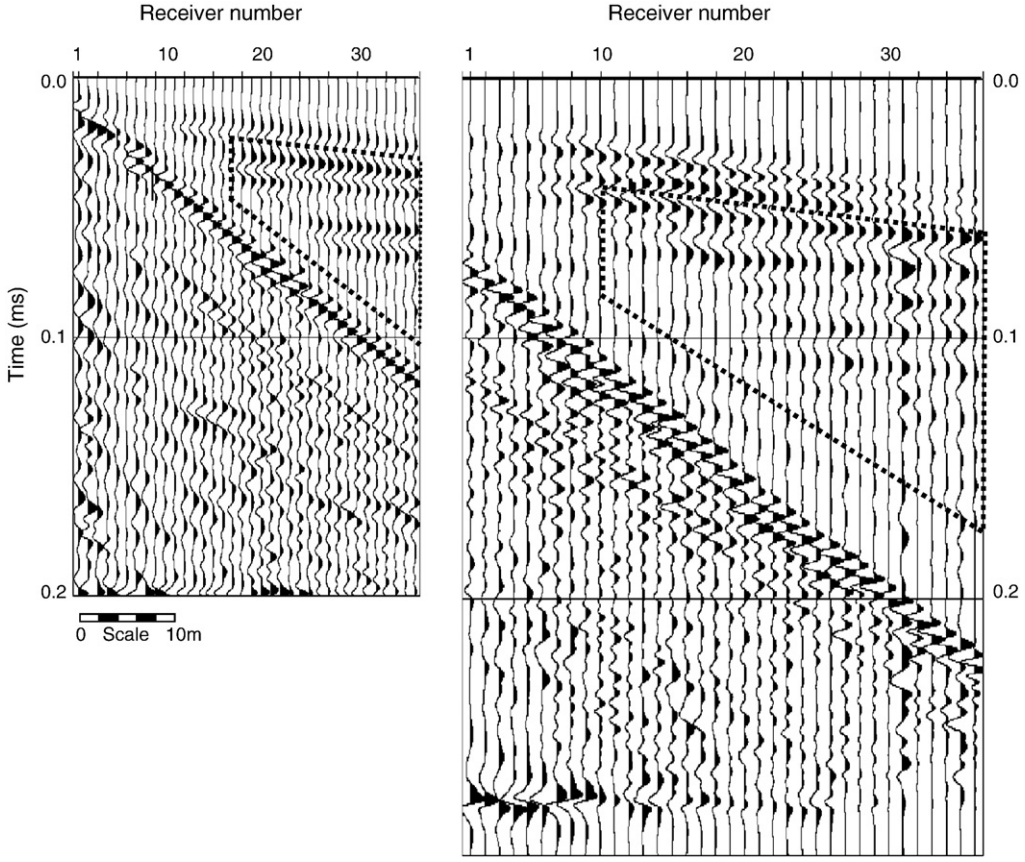

Fig. 11. P-wave shots of seismic reflection P1 line (left) acquired with sensors offset of 1 m and P2 line (right) acquired with sensors offset of 1.5 m. The data were muted outside of dot line.

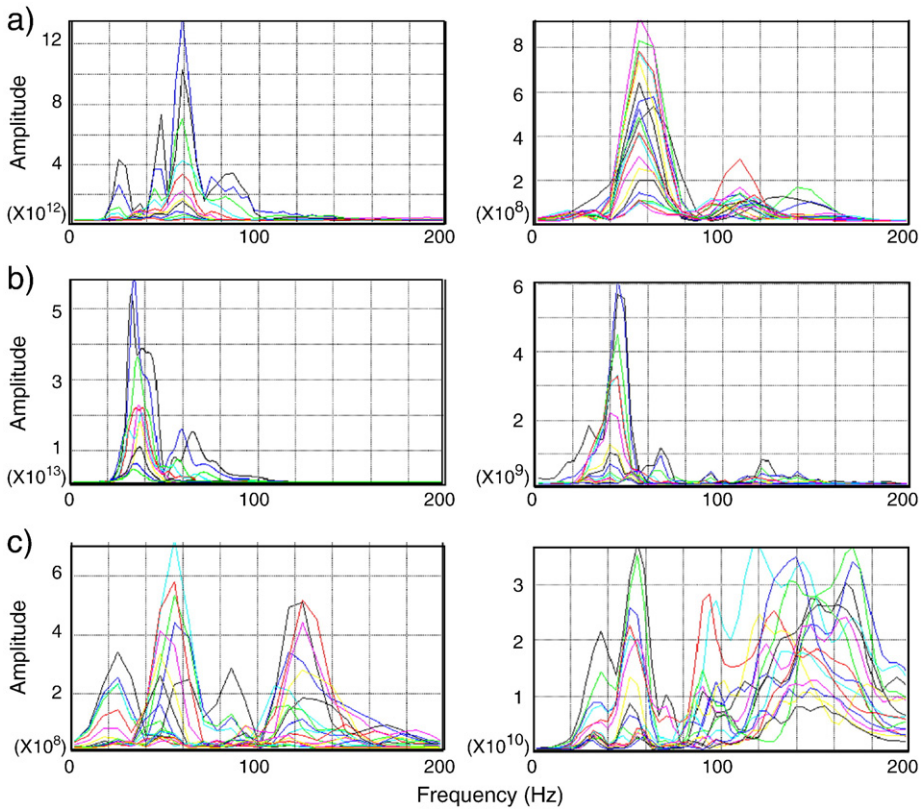

Fig. 12. Spectral analysis of a P1 wave shot (left) and of a P2 shot (right). On the top spectral analysis of shot, noise in the middle and signal on the bottom. Frequency of 150–180 Hz and velocity of 2000 m/s gives a vertical resolution (Rayleigh criterion of $\lambda/4$) of 2.8 m.

4.2.4. PS-wave seismic reflection

The PS data were processed following the flow chart of Fig. 14. The typical step processing, which consists of polarity reversal of the trailing spread and rotation of the horizontal components, was skipped because the receivers used in the survey were single-component and the acquisition geometry was off-end. The processing parameters were based on the field data analyses described below. Shots show a good signal-to-noise ratio in the polygonal area (Fig. 15). The shot spectral analyses (Fig. 16a) show frequencies from 15 to 55 Hz for amplitude ratios > −15 dB. The noise has frequencies with amplitudes > −14 dB up to 30 Hz and signals up to 50 Hz. Taking into account the former frequency and a

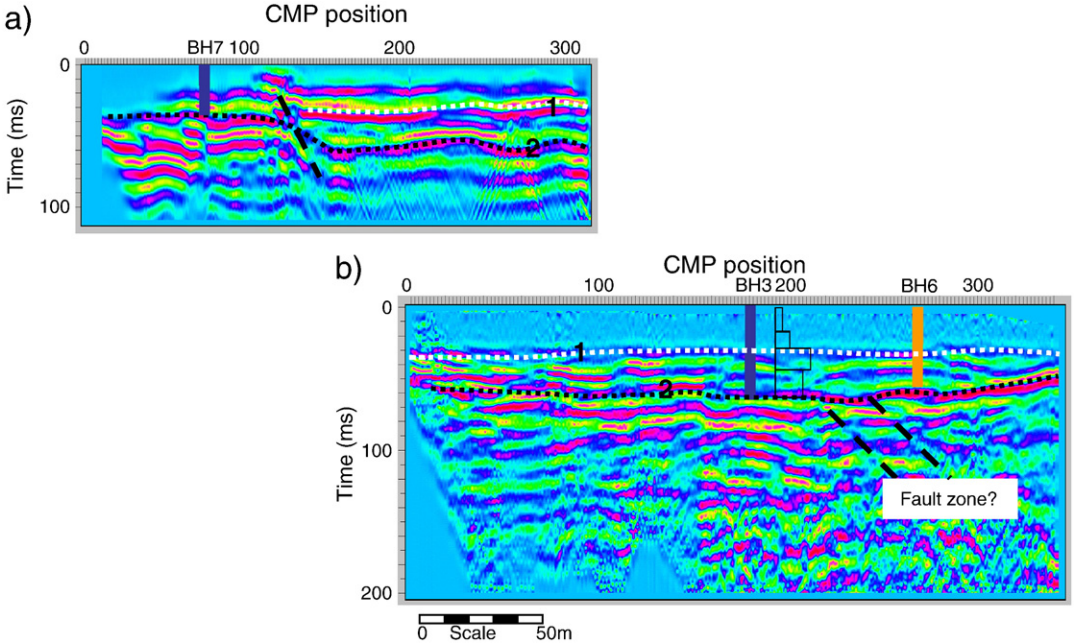

Fig. 13. Stack sections of P1 and P2 lines. White dotted line (1) draws the top of gravel sandy layer and black dotted line (2) the top of limestone formation detected by boreholes BH7 and BH3. Two-way travel time P-wave seismic profile in Fig. 10b is drown near the BH3.

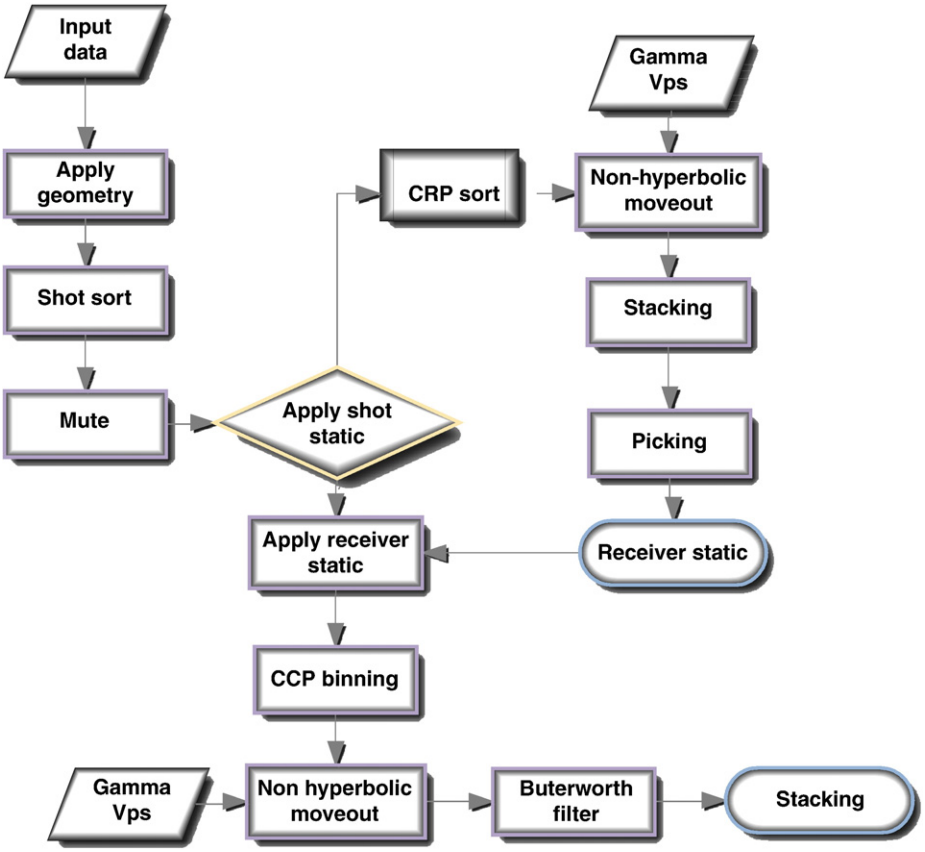

Fig. 14. Flow of PS-wave processing.

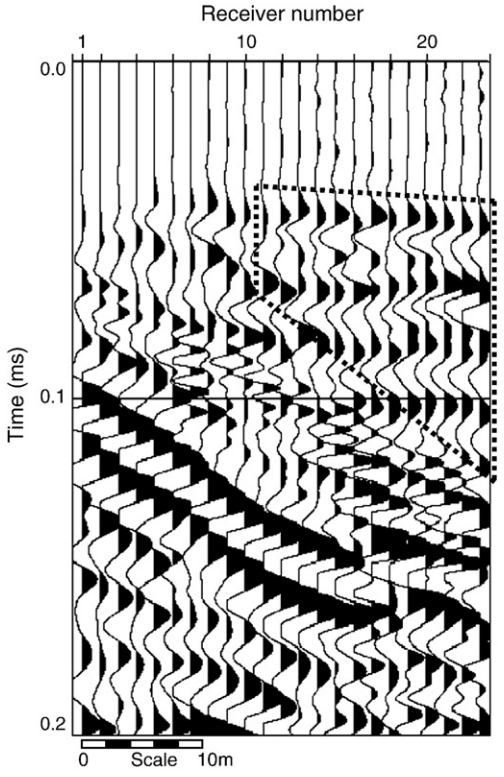

Fig. 15. PS-wave shot acquired with sensors offset of 1.5 m. The data were muted outside of dot line.

S-wave velocity of 800 m/s, the waiting resolution (Rayleigh criterion of $\lambda/4$) is about 4 m.

A Butterworth filter (50–200 Hz) was applied to remove the noise. Because of the low signal-to-noise ratio (Figs. 15 and 16), mainly due to the high energy of the ground roll, special care was given to the muting and to the static correction. For this reason, a severe muting was applied to the shot, leaving only the energy within the polygonal area of Fig. 15.

The static correction was performed by separately considering the shot and receiver static (Cary and Eaton, 1993; Chan Wai-kin, 1998); the static source was determined from the refraction survey, and the static receiver was calculated from the common receiver stacked sections (CRP). In detail, it was performed in the following way: 1) application of the shot static to the data; 2) sorting of common receiver; 3) non-hyperbolic NMO correction; 4) hand-picking of the CRP-stacked section of a single continuous event on the receiver stack section; 5) computation of mean/average pick time and subtraction of the actual time pick; and 6) the static corrections, smoothed with a moving average mean of four samplings, were applied back to the CRP-stacked section to check the result until a satisfactory solution was obtained. To obtain the final static solution, this process was iterated several times.

Based on the considerations outlined in the introduction to PS data, the ACCP sorting approximation (Fromm et al., 1985) was used with the objective of focusing the layers of the first 20 meters.

ACCP binning was performed with the Constant Gamma Stack step and a non-hyperbolic NMO correction. The first value of gamma used in the iterative process was selected from P and S velocities obtained from seismic refraction and MASW surveys.

Finally, for display purposes, an automatic gain-control (AGC) function was applied to the data (Fig. 17a).

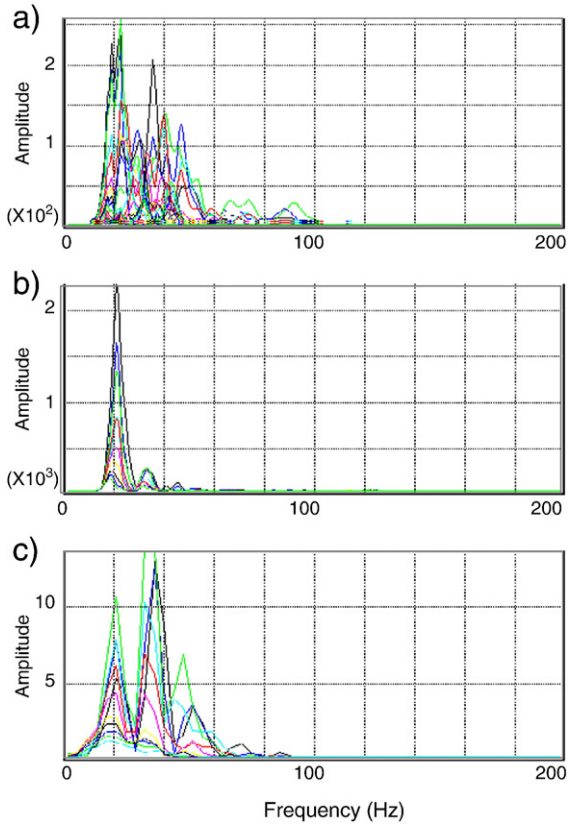

Fig. 16. Spectral analysis of PS-wave shot (a) noise (b) and signal (c).

The PS stack section (Fig. 17a) shows only a continuous reflection at 40 ms depending on the use of ACCP sorting instead of a CCP sorting, which only focused this reflector. Comparing the stack section with the two travel time velocity profiles of the PS-wave shown in Fig. 10d and drown on the right in Fig. 17a, we observe that the dotted white reflection corresponds to the top of compacted gravel and sand as detected by boreholes.

4.2.5. Joint data interpretation

The analysis of processed data shows that each method can investigate different depths depending on acquisition parameters and their own intrinsic physical parameters, confirming that the underground reconstruction in terms of features and velocity profiles is possible only from the joint interpretation of more data based on principles and/or different physical parameters. An important rule is given by borehole stratigraphy, which allows the thickness and lithologies to be constrained both in the data inversion and interpretation.

In this paper, the VES and ERT data have provided information on features and formation types; seismic data have provided on the features and on P and S velocities; and boreholes have allowed the thickness in the data inversion to be constrained and the geophysical layers of the first 50 m to be characterised in terms of lithologies. This setting up to limestone bedrock is well shown by the VES and ERT data in Fig. 6, which has allowed the electro-stratigraphy to be carried out along a 2D profile normal to the valley axis. Correlation of resistive data with boreholes has allowed the association to be made between each resistivity and lithology up to 50 m. In the centre of the valley, the resistive data resulted in detection of a resistive layer 2 (Fig. 6) overlapping a conductive layer, which was not lithologically defined due to the lack of boreholes in this area. More information about this body and the elastic characteristics of near-surface formations were determined from seismic data. The refraction data have provided an indication of the features and allowed the velocity profiles of the P-waves of the formations to be defined for the first 12–15 m, corresponding to the top of the compacted sandy-gravel layer. By relating the velocities determined from the refraction data and MASW with stratigraphy of BH3, the two-way travel time profiles of P and S velocity were calculated for the formations up to the limestone

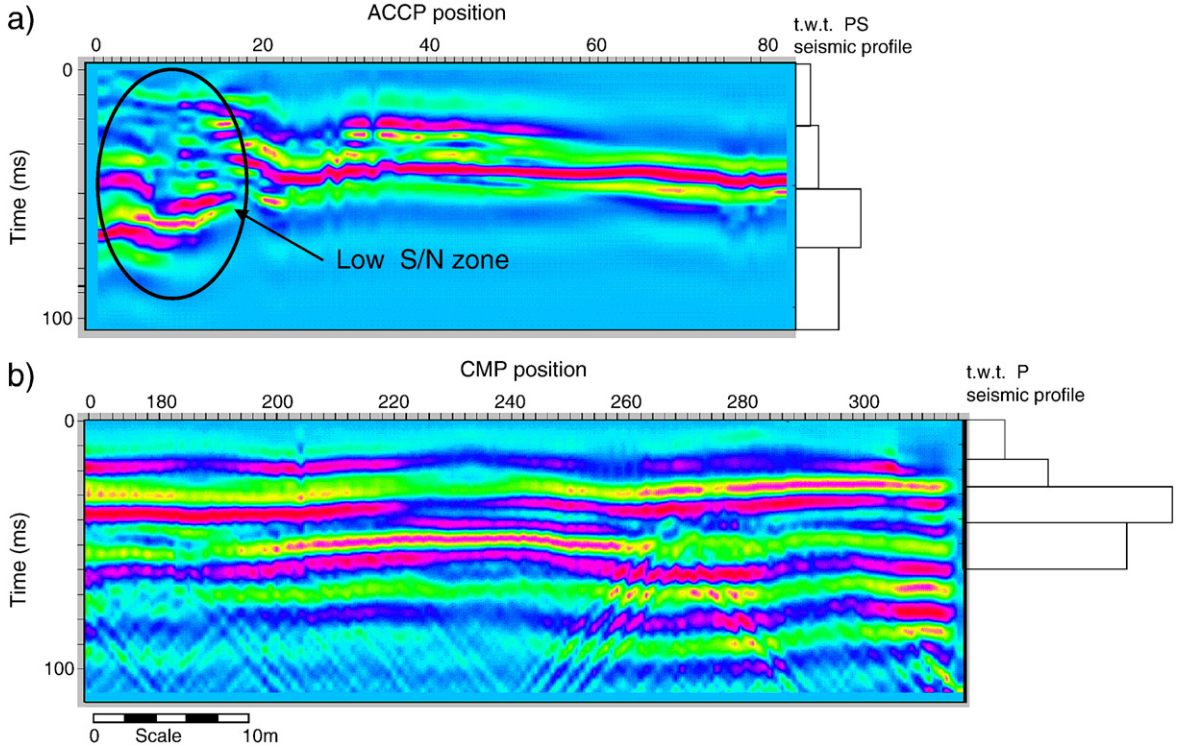

Fig. 17. PS (a) and P (b) stack sections. White dotted line draws the gravel sandy top layer. On the left of profiles, t.w.t. of PS and P-waves are drown.

(Fig. 10). The P and S velocity profiles were used in the seismic reflection data inversion as starting parameters in the iterative processes, and they were used to calculate the two-way travel time profiles, which were used for the interpretation of reflections in terms of lithologies.

Based on the joint interpretation of seismic reflection profiles, VES and ERT data show a good overlapping between the top of resistive bodies 1 and 2 of Fig. 6 and reflection 2 of Fig. 13, which appears continuous along the whole profile, even if the reflection in correspondence with resistive body 2 appears more continuous than in the other zone. Combining information from the VES, which indicates that the resistive body 2 overlaps a clay formation, and information from seismic data, which suggests that this body is composed of limestone, we can advance the hypothesis that the body 2 could be a detached limestone formation.

Therefore, the geologic section of Fig. 4 in the centre of the valley must be revisited in light of the geophysical data.

5. Conclusion

This study has proven that the joint interpretation of seismic data with vertical electrical sounding and electrical resistivity tomography constrained by borehole stratigraphies are useful tools for reducing the ambiguity in feature reconstruction and for determining P- and S-wave profiles of near-surface formations (<50 m). Even if the data inversions of each method were performed separately, the constraints on layer thickness and velocities determined from boreholes and seismic refraction allowed the ambiguity in data inversion to be reduced. For example, in the case study referred in this paper, vertical electric soundings, electrical resistivity tomography and boreholes have helped to confirm the depth of reflectors, while seismic refraction and MASW data have resulted in *a priori* information on the velocities, which were used to determine the static correction and the velocity profiles for P and PS data processing.

Depending on the methods, different depths were investigated. The vertical electrical sounding and electrical resistivity tomography methods allowed the reconstruction of the underground features up to limestone, and the seismic data provided information on the P and S velocity profiles and the features of strata.

Because of velocity inversion at the contact of the bottom of the sandy-gravel layer with the top of clay, the seismic refraction method allowed investigation of only the first 9–12 m of the underground, but the velocities carried out from the inversion combined with borehole stratigraphies allowed determination of the P-wave velocity profile and the delay time for the seismic reflection static computation.

MASW data provided the S velocity profile up to limestone. The uncertainty in the MASW data inversion was reduced using borehole stratigraphy. The P and S two-way travel time profiles obtained from seismic refraction and MASW data were very useful tools in data inversion and interpretation of P and PS seismic reflection data.

P and PS seismic data have shown to be effective in the reconstruction of near-surface formation, even if obtaining this data involves greater investments in data acquisition. The good quality of seismic data depends on the signal-to-noise ratio, which can be improved by creativity in the acquisition and processing phases. A good signal-to-noise ratio is available only in the window out of the ground roll cone, and a drastic muting in the processing phase that eliminates energy inside such cones is necessary for improving the signal-to-noise ratio. This requires a wide-shot geophone offset to be used during acquisition, keeping in mind that for the superficial zone, the optimum window changes very quickly with the offset. In the processing of converted PS waves, it is important to take into account that the use of ACCP sorting is based on the lack of dependence of CCP with the offset. This approximation is correct only for depths greater than the shot-receiver offset. For shallower depths, the ACCP sorting does not change with depth, and it therefore does not allow reflections to be focused throughout the entire time window.

We must stress that for small depths it is very difficult to obtain a correct correlation of stack section with boreholes due to the errors that occur in the depth-to-time conversion. In this case, the seismic reflection and MASW profiles obtained with the correlation of borehole stratigraphy allow the problem to be bypassed.

Acknowledgments

I would like to thank Rita de Nardis, Paolo Marsan and Giuliano Milana for their valuable discussion about this work and Italian Civil Protection for providing the boreholes and VES field data.

References

Bernabini, M., 1965. Alcune considerazioni sui rilievi sismici a piccolo profondità. Bollettino di Geofisica Teorica ed Applicata II (26), 106–118.
Bernabini, M., Cardarelli, E., 1997. Variable damping factor in travel time tomography. Journal of Applied Geophysics 38, 131–141.
Cardarelli, E., Cercato, M., Di Filippo, G., 2007. Assessing foundation stability and soil structure interaction through integrated geophysical techniques: a case history in Rome Italy. Nears Surface Geophysics 5, 141–147.
Carr, B.J., Hajnal, Z., 1999. P- and S-wave characterization of near-surface reflectivity from glacial tills using vertical seismic profiles. Geophysics 64 (3), 970–980.
Carr, B.J., Hajnal, Z., Prugger, A., 1998. Shear-wave studies in glacial till. Geophysics 63 (4), 1273–1284.
Cary, P.W., Eaton, W.S., 1993. A simple method for resolving large converted-wave (P-SV) statics. Geophysics 58 (3), 429–433.
Chan Wai-kin, 1998. Analyzing Converted-Wave Seismic Data: Statics, Interpolation, Imaging and P-P Correlation. Ph. D. Thesis. Calgary, Alberta.
Deidda, G.P., Balia, R., 2001. An ultra shallow SH-wave seismic reflection experiment on a subsurface ground model. Geophysics 66 (4), 197–1104.
Domenico, S.N., 1974. Effect of water saturation on seismic reflectivity of sand reservoirs encased in shale. Geophysics 39, 759–769.
Feroci, M., Orlando, L., Balia, R., Bosman, C., Cardarelli, E., Deidda, G., 2000. Some consideration on shallow seismic reflection surveys. Journal of Applied Geophysics 45, 127–139.
Fromm, G., Krey, T., Wiest, B., 1985. Static and dynamic corrections, seismic shear waves. Handbook of Geophysical Exploration, 15a. Geophysical press, pp. 191–225.
Gardner, L., 1939. An area plan of mapping subsurface structure by refraction shooting. Geophysics 4, 247–250.
Garotta, R., Granger, P.Y., 1988. Acquisition and processing of 3Cx3D data using converted waves. 58th Annual International Meeting. SEG, pp. 995–997. Expanded Abstract.
Harris, J.B., Miller, R.D., Xia, J., Hunter, J.A., Park, C.B., Laflen, D.R., Good, R.L., 2000. Near-surface shear wave reflection surveys in the Fraser River delta, B.C., Canada. SEG.
Hilterman, F.J., 2001. Seismic amplitude Interpretation. : Distinguished Instruction Short Course SEG, EAEG, Houston-Usa.
Hunter, J.A., Burns, R.A., Good, R.L., MacAulay, H.A., Gagnè, R.M., 1982. Optimum field technique for bedrock reflection mapping with the multichannel engineering seismograph. In Current Research, Part B; Geol.Surv. Can., Paper 82–1B, 125–129.
Hunter, J.A., Benjumea, B., Harris, J.B., Miller, R.D., Pullan, S.E., Burns, R.A., Good, R.L., 2002. Surface and downhole shear wave seismic methods for thick soil site investigations. Soil Dynamics and Earthquake Engineering 22, 931–941.
Iverson, W.P., Fahmy, B.A., Smithson, S.B., 1989. Vp/vs from mode-converted P-SV reflections. Geophysics 66, 97–109.
Li, Xinxiang, Lu, Han-xing, 1999. Revisiting the fold discontinuity after ACCP binning. : CREWES Research Report, vol. 11.
Nazar, Brad. 1991. An interpretive study of multicompontent seismic data from the Carrot Creek area of west–central Alberta. M.Sc. 1991. (Canadian theses number: ISBN 0315751398) QE471.15.C6 N39 1991.
Orlando L., Bonci L., Calcaterra S., de Nardis R., Eulilli V., Ferri F., Marsan P., Milana G., Raoli F. 2003. Interpretazione integrata di dati geofisici per la valutazione della risposta sismica dei sedimento della conca L'Aquila-Scoppito. Extented abstract, 4° Forum Italiano di Scienze della Terra, Belluria,16–18 settembre 2003.
Rix, G.J., Lai, C.G., Spang, A.W., 2000. In situ measurement of damping ratio using surface waves. Journal of Geotechnical and Geoenvironmental Engineering 126 (5), 472–480.
Schafer A.W., 1993. Binning, Static Correction, and Interpretation of P-SV Surface-seismic data. M. Sc. Thesis. Calgary, Alberta.
Socco, L.V., Strobbia, C., 2004. Surface-wave method for near-surface characterization: a tutorial. Near Surface Geophysics 2, 165–185.
Tallini, M., Magaldi, D., 2002. Schema geo-litologico della piana quaternaria L'Aquila-Scoppito. Geoingegneria ambientale e mineraria, A 39 (1).
Tessmer, G., Behle, A., 1988. Common reflection point data-stacking technique for converted waves. Geophysical Prospecting 36, 671–688.
Thomsen, L., 1999. Converted-wave reflection seismology over inhomogeneous, anisotropic media. Geophysics 64 (3), 678–690.

Xia, J., Miller, R.D., Park, C.B., 1999. Estimation of near-surface shear wave velocity by inversion of Rayleigh waves. Geophysics 64, 691–700.
Yang J., 2003. Numerical and physical modelling of P-S converted waves in VTI media. M. Sc. Thesis. Calgary, Alberta
Yilmaz, O., 2001. In: Doherty, S.M. (Ed.), Seismic data analysis, vol. 2. Society of Exploration Geophysicist.
Young, R.A., Hoyos, J., 2001. Near Surface SH waves surveys in unconsolidated, alluvial sediments. Leading Edge 936, 948 September 2001.
Yuan, J., Li, X.Y., 1997. Converted-wave CCP binning and velocity analysis. Processing Three-Component Seafloor Seismic Data. Edimborough University.
Zhang, Y., 1996. Nonhyperbolic converted wave velocity analysis and normal move out. 62nd Ann. Internat. Mtg., Soc. Expl. Geophys, pp. 1555–1558. Expanded Abstracts.
Zhang, Y., Robinson, E.A., 1992. Stacking P-SV converted wave data with raypath velocity. 62nd Ann. Internat. Mtg., Soc. Expl. Geophys, pp. 1214–1217. Expanded Abstracts.